SCIENCE CHINA
Chemistry

•ARTICLES•

April 2022 Vol.65 No.4: 733–739
https://doi.org/10.1007/s11426-021-1213-2

From *n*-alkane to polyacetylene on Cu (110): Linkage modulation in chain growth

Zhengming Hao[1†], Junjie Zhang[1†], Miao Xie[1†], Xuechao Li[1], Lina Wang[1], Ye Liu[1], Kaifeng Niu[1,2], Junbo Wang[1], Luying Song[1], Tao Cheng[1], Haiming Zhang[1] & Lifeng Chi[1*]

[1]*Institute of Functional Nano and Soft Materials (FUNSOM) and Jiangsu Key Laboratory for Carbon-Based Functional Materials and Devices, Soochow University, Suzhou 215123, China;*
[2]*Department of Physics, Chemistry and Biology, Linköping University, Linköping 58183, Sweden*

Received November 15, 2021; accepted February 15, 2022; published online February 28, 2022

Direct coupling or transformation of inert alkanes based on the selective C–H activation is of great importance for both chemistry and chemical engineering. Here, we report the coupling of polyenes that are transformed from *n*-dotriacontane (*n*-$C_{32}H_{66}$) through on-surface cascade dehydrogenation on Cu (110) surface, leading to the formation of polyacetylene (PA). Three distinct linkages have been resolved by scanning tunneling microscope (STM) and noncontact atomic force microscope (nc-AFM). Apart from the α-type linkage which is the stemless coupling of the terminal C–C double bond in *trans*-configuration, β- and γ-type linkages appear as knots or defects which are, in fact, the C–C couplings in *cis*-configurations. Interestingly, the "defects" can be effectively suppressed by adjusting the surface coverage, thus making it of general interest for uniform structure modulation.

on-surface chemistry, scanning tunneling microscope, *all-trans* polyacetylene, linkage, chain growth

Citation: Hao Z, Zhang J, Xie M, Li X, Wang L, Liu Y, Niu K, Wang J, Song L, Cheng T, Zhang H, Chi L. From *n*-alkane to polyacetylene on Cu (110): Linkage modulation in chain growth. *Sci China Chem*, 2022, 65: 733–739, https://doi.org/10.1007/s11426-021-1213-2

1 Introduction

Polyacetylene (PA) is the first synthesized conductive polymer showing unique electrical and mechanical properties [1–5]. Although the structural unit is simple, the control of molecular weight and stereochemistry of PA chains is challenging *via* conventional acetylene polymerization pathway [6–9]. PA with alternating single and double bonds can stay in *trans*- or *cis*-configuration but practically in the *cis-trans* mixture. The *all-trans* conjugated PA is more stable and more conductive than *cis*-PA or their mixture [10–16]. Meanwhile, the controlled synthesis of single-configuration polyacetylene chains could provide an ideal template for the study of conducting polymers and open up broad prospects for the construction of functionalized molecular pads in organic electronics/semiconductors [17–19]. Although the modulation on *cis-trans* configurations in PA is achieved by the designing and processing at molecular level, it still remains a challenge to obtain *all-trans* PA.

The newly developed on-surface chemistry provides promising possibilities for synthesizing precise molecular nanostructures that are not accessible in solution chemistry [20–29], including the preparation of *all-trans* single-chain polyene with predictable length transformed from *n*-alkane [30]. On-surface chemistry also provides the possibility to modulate the structural uniformity by fine-tuning precursor structure, surface diffusion, molecular preorganization and so on [21–34].

Herein, we report the coupling of polyenes with uniform

†These authors contributed equally to this work.
*Corresponding author (email: chilf@suda.edu.cn)

length, which are transformed from *n*-dotriacontane (*n*-$C_{32}H_{66}$) through the dehydrogenation on a Cu (110) surface, leading to the formation of polyacetylene (PA). Linear *all-trans* polyenes tend to react with each other, forming oligomers with three distinct linkages corresponding to their connection in different *trans*- and *cis*-configurations, as characterized by STM and nc-AFM. Significantly, we are able to modulate the ratio between the three linkages by altering the thermal treatment procedures and controlling the surface coverage. In particular, changing the surface coverage turns out to be an efficient way to regulate C–C coupling linkages, thus reducing the defects in the chain growth process.

2 Experimental

2.1 STM measurements

STM measurements were conducted in a commercial scanning tunneling microscope (Unisoku Ltd., Japan) under ultrahigh vacuum conditions at a base pressure lower than 1.0×10^{-10} Torr. All STM pictures (unless otherwise stated) were acquired at 77 K with the usage of an electrochemically etched tungsten tip. The Cu (110) single crystalline was purchased from a commercial company (Mateck, Germany) and cleaned with several rounds of the standard sputtering-annealing process before utilization. The *n*-dotriacontane molecules (98%) were obtained from J&K Scientific Ltd. and used directly without further purification. The processing and analysis of STM images were performed *via* the WSxM software [35]. Organic molecular beam deposition was conducted at a sublimation temperature of 370 K by a commercial three-cell UHV evaporator (Kentax, Germany). The temperature of the metal surface was measured by an infrared thermometer (Japan sensor corporation), showing a slight deviation from the real temperature due to inherent technical problems and background infrared-signal noise.

2.2 AFM Measurements

The constant-height nc-AFM experiments were conducted in a commercial LT-STM (Scienta Omicron, Germany) operated at 4.6 K under a base pressure of 1.0×10^{-11} mbar. A tuning fork q-plus sensor with a tungsten tip (resonance frequency $f_0\approx25.6$ kHz, a quality factor $Q>10{,}000$ and oscillation amplitude $A=70$ pm in the constant-height mode) was grounded to increase the stability of the system. The attached tungsten tip was cleaned under cycles of applied voltage and sharpened *via* the indentation into a clean Cu (111) surface for CO termination [36]. The tip-height offsets (ΔZ) for constant-height AFM images were defined as the offset in the tip-sample distance relative to the STM set point as stated, with positive (negative) values indicating that the tip-sample distance increased (decreased) with respect to the STM set point. The Cu (110) crystal was prepared through cycles of sputtering and annealing up to 800 K. The molecules were evaporated onto the substrate held at room temperature using a commercial Knudsen cell from Kentax.

2.3 DFT calculation

The quantum mechanics (QM) calculations were carried out using the VASP software, version 5.4.4 [37–39]. We used the Perdew, Burke and Ernzerhof (PBE) flavor [40] of density-functional theory (DFT) with the post-stage DFT-D3 method to correct London dispersion (van der Waals attraction) with Becke-Johnson damping [41]. The projector augmented wave (PAW) method [42,43] was used to account for core-valence interactions. The kinetic energy cutoff for plane wave expansions was set to 400 eV, and reciprocal space was sampled by the Γ-centered Monkhorst-Pack scheme with a grid of 3×3×1. In this work, we carried out simulations for the Cu (110) model, which was modeled by a 4×8 unit cell with three periodic atom layers. During the geometry optimizations, the atoms in the bottom layer were fixed at their bulk positions, whereas the rest of the atoms were allowed to relax. The vacuum layer is at least 20 Å above the surface. The convergence criteria are energy differences of 1×10^{-5} eV for solving the electronic wave function. The Methfessel-Paxton smearing of the second order with a width of 0.2 eV was applied. All atomic coordinates converged to 3×10^{-2} eV Å^{-1} for maximal components of forces. The climbing-image nudged elastic band (CI-NEB) method [44,45] with six intermediate images was employed to investigate the moving reaction barrier.

3 Results and Discussion

Figure 1a displays a representative STM image after initial deposition of *n*-$C_{32}H_{66}$ on a Cu (110) substrate at room-temperature (RT). The lamellar structure with a constant width that is similar to the self-assembly of *n*-$C_{32}H_{66}$ on other surfaces [33]. The magnified STM images show detailed arrangement of the *n*-$C_{32}H_{66}$ on Cu (110), indicating a shoulder-to-shoulder packing manner (Figure S2) with the long-axis of the molecule perpendicular to [001] direction. Moreover, due to the incommensurate periodicity between the *n*-$C_{32}H_{66}$ and underlying Cu (110) lattice, the *n*-$C_{32}H_{66}$ lamellae exhibit an undulated topography as discussed in our previous paper [30], known as Moiré patterns [46–48].

Annealing the sample to ~450 K results in the dehydrogenation of *n*-alkane, leading to the transformation of the alkanes to the corresponding *all-trans* polyenes (Figure 1b), as reported in our previous work [30]. At this stage, polyenes are mostly monodispersed, with only a few of them coupled.

Further annealing to ~470 K leads to the interconnection of the polyenes (Figure 1c). However, in the close-up STM image (inset of Figure 1e and 1f), we can easily find that the connections between the polyenes are not uniform but exhibit randomly distributed knots. The coupling happens between the molecules located both in the same and the neighbor copper spines along [1$\bar{1}$0] direction, which differs from the C–C coupling observed on the Au (110) surface reported previously [31]. Since the STM images cannot provide the bond resolution for those knots, high-resolution non-contact AFM (nc-AFM) measurements were conducted to gain further information. We can then classify the linkages into three major categories denoted as α-, β-, γ-type, as illustrated in Figure 1d–f. The α-type linkage is a perfect connection between polyenes (Figure 1d). In this case, the position of the linkage cannot be directly recognized but only be deduced from the length of the oligomers divided by the length of the *n*-$C_{32}H_{66}$ monomer, *i.e.*, 4 nm. As for β-type linkage, both STM and nc-AFM images reveal obvious deviations from the perfect connection. There are protrusions in the coupled chain in the STM image (Figure 1e), which is determined to be the *cis*-isomerism with the nc-AFM image. The connected polyenes are in the same spine of Cu (110). By contrast, the γ-type linkage is also the connection between polyenes in *cis*-configuration but forming cross-groove coupling (Figure 1f). Notably, we observe some twisted coupling at the *trans*-PA terminal in Figure 1c, which might be attributed to the formation of a ring-like structure reminiscent of benzene or larger rings during annealing. Increasing the annealing temperature or prolonging the annealing period of *trans*-PA/Cu(110) samples may increase the amount of such termini [49,50], which will be further confirmed in the future work.

As mentioned in the introduction, the mixture of *trans-cis* configuration in PA will significantly influence its properties. It is thus of great interest to modulate the ratio of the three linkages in our system. Experimentally, we can regulate the linkages in two ways, *i.e.*, altering the annealing procedure or changing the initial surface coverage. In the first approach, we tried to adjust the annealing temperature, annealing time and their combination. When the annealing temperature is below ~470 K or the annealing time is insufficient at a higher temperature, the surface is dominated by a partial alkane-polyene mixture and polyene dimer (Figure S3). Among the dimers, α- and β-type linkages are predominant. When the annealing temperature is above 470 K and the annealing time

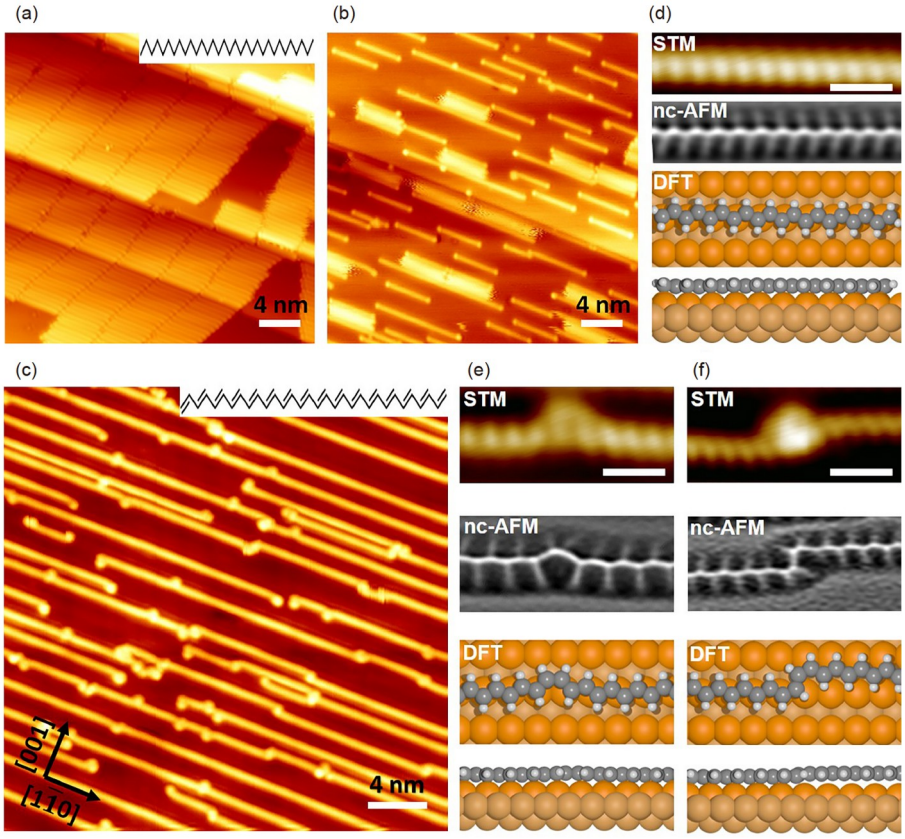

Figure 1 Self-assembly, transformation and coupling of *n*-$C_{32}H_{66}$ on Cu (110) with an initial coverage of 0.4 monolayers (ML). (a) STM image of 0.4 ML *n*-$C_{32}H_{66}$ evaporated on clean Cu (110) held at room temperature. Inset gives the structural model of *n*-$C_{32}H_{66}$. (b) Representative STM image after annealing at 450 K for 30 min. (c) Representative STM image after annealing at 470 K for 60 min. Scanning conditions (a–c): I_t=20 pA, V_t=−1.0 V. (d–f): STM, nc-AFM image and top- as well as side-view DFT models in α-, β-, γ-type linkages. Image size: (d) 2.6 nm×0.4 nm; (e) 1.7 nm × 0.5 nm; (f) 2.4 nm×0.5 nm. Scanning conditions of (d–f): I_t = 3 pA, V_t = 200 mV (color online).

is extended, the reactants react sufficiently to form one-dimensional (1D) PA chains with randomly distributed linkages. In the second approach, we keep the same annealing temperature (above 470 K) and the same annealing time but vary the initial coverages (0.1, 0.4 and 0.8 ML) (Figure 2). Statistical analysis (see more details in Figure S4 and Table S1) on the linkages indicates that the portion of both β- and γ-type linkages decreases while the portion of α-type linkages increases.

To understand such coverage-dependent linkage modulation, we have to take the preorganization of the molecules into consideration. It is known that *n*-alkane can form the same enantiomeric and anti-enantiomeric packing due to its zigzag carbon skeleton configuration, as illustrated in Figure 3a. Increasing the surface coverage of *n*-alkane does not lead to phase transformation of the self-assembled structure but reduces the distance between the self-assembled lamellae, thus affecting the connection of polyene monomers concerning "chirality" selection in the subsequent annealing process. The *all-trans* polyenes transformed from *n*-alkanes mainly keep the mirror symmetry following the preorganization of the *n*-alkanes, which can be defined as lift hand ("*L*") and right hand ("*R*"), respectively (Figure 3a). The α-type linkage leads to the perfect *all-trans* PA, which is coupled by the same polyene monomer along the same ridge in "*L*" or "*R*". The β-type linkage might be generated through the coupling of different polyene monomers in "*L*" and "*R*" or directly undergo *trans-cis* isomerism under thermal treatment. The γ-type linkage of PA is formed by coupling the polyene in "*L*" or "*R*" across the grooves (Figure 3b).

At the low-coverage stage, the self-assembled lamellae of *n*-$C_{32}H_{66}$ are widely spaced. Almost no interaction between molecular lamellae in the [1$\bar{1}$0] direction implies that the adsorption-induced surface enantiomers are randomly distributed at this coverage (Figure 4a). Since the adsorption mirror symmetry of polyenes is mainly determined by the corresponding *n*-alkane after transformation, the enantiomer of the polyene monomers will also become randomly distributed after annealing. Theoretically, the proportion of α- and β-type linkages should be essentially equal at this state, but the statistics show that the portion of α-type linkages is higher. This result implies that *all-trans* PA has lower migration energy barriers than *cis*-PA or their mixtures on the surface and is proved by DFT calculations (Figure S5),

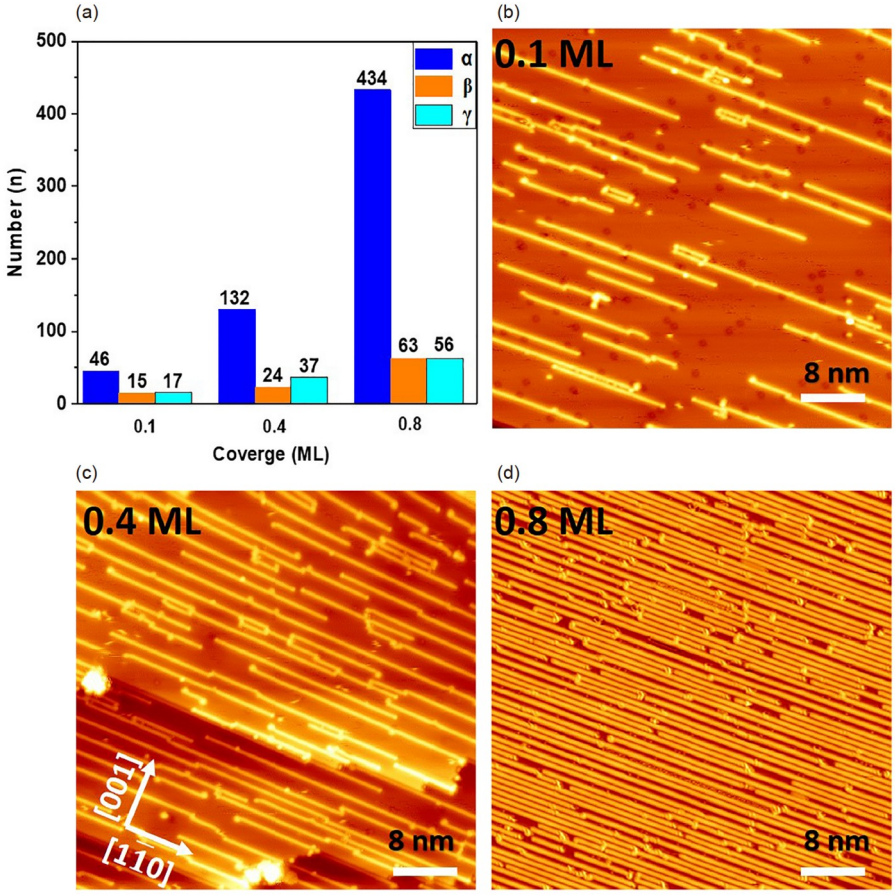

Figure 2 Regulation and statistics of linkages at different surface coverages. (a) Statistical diagram of three linkages at different coverages. (b–d) Expanded STM images of the Cu (110) surface after annealing at 470 K with an initial coverage of 0.1, 0.4, and 0.8 ML *n*-$C_{32}H_{66}$ molecules, respectively. Scanning conditions: I_t=20 pA, V_t=−1.0 V for (b) and (c); I_t=200 pA, V_t=−1.0 V for (d) (color online).

which increases the probability of collision between polyenes with the same enantiomeric adsorption and leads to a higher proportion of α-type linkages. With increased surface coverage, self-assembled *n*-$C_{32}H_{66}$ lamellae gradually evolved into a tight stacking of double or multiple rows in the [1$\bar{1}$0] direction (Figures 4b and 4c). As observed experimentally, the adjacent lamellae in compact self-assembly of *n*-$C_{32}H_{66}$ are mostly arranged in the [001] direction with the

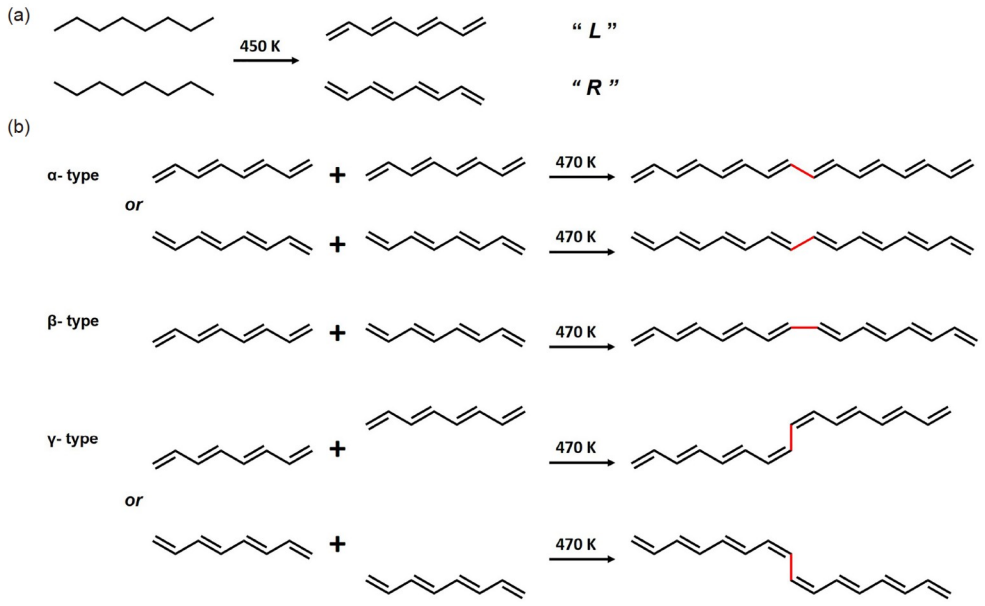

Figure 3 Schematic illustration of the coupling reaction of *n*-$C_{32}H_{66}$ on Cu (110). (a) The transformation of *n*-alkane to *all-trans* polyenes at ~450 K. "*R*" and "*L*" represent polyene monomers with different adsorption configurations, respectively. (b) Schematic diagram of polyacetylene formation of three connection modes (color online).

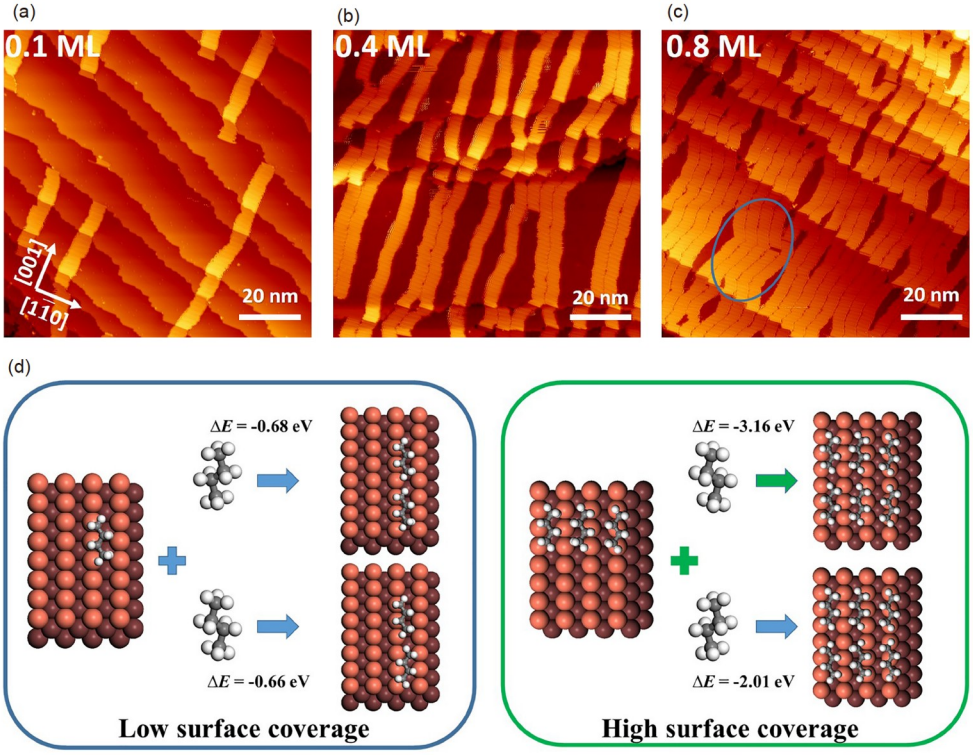

Figure 4 STM image and adsorption energy of self-assembly of *n*-$C_{32}H_{66}$ at different coverages. (a–c) The self-assembly diagrams of *n*-$C_{32}H_{66}$ at 0.1, 0.4, and 0.8 ML, respectively. Scanning conditions: I_t=20 pA, V_t=−1.0 V for all. (d) The adsorption energy of molecules with the same enantiomeric adsorption and anti-enantiomeric adsorption at different coverage (color online).

same chirality, as indicated with blue circles in Figure 4c. According to the principle that the self-assembled molecules should keep the lowest Gibbs free energy, we further performed the DFT calculation on the adsorption energy of alkanes for both packing. The calculation results in Figure 4d show that the energy of alkanes with the same enantiomer adsorption decreases with the increase of surface coverage area. Under low surface coverage, the adsorption energy of alkanes adsorbed with the same enantiomeric and anti-enantiomeric structure is very close (−0.68 and −0.66 eV, respectively), which can explain the random adsorption configuration of alkanes under low surface coverage. However, with the increase of coverage, the adsorption energy of alkanes with different structures changes significantly: the adsorption energy of alkanes with the same enantiomer adsorption configuration is −3.61 eV, while that of alkanes with the anti-enantiomeric adsorption configuration is −2.01 eV. The calculated results show that the proportion of adsorption configurations of the same enantiomeric increases with the increase of surface coverage, which provides a reasonable interpretation for the increased portion of the α-type linkage with increased surface coverage.

To verify the linkage modulation mechanism in the chain growth, we further calculated the migration of polyene monomers with different chain lengths on substrates (Figure 5). In the [1$\bar{1}$0] direction, the corresponding energy barriers of C_4H_6, C_6H_8, C_8H_{10} and $C_{10}H_{12}$ are 0.225, 0.275, 0.305 and 0.301 eV, respectively (Figure 5a). In the [001] direction, the corresponding energy barriers of C_4H_6, C_6H_8, C_8H_{10} and $C_{10}H_{12}$ are 0.951, 1.370, 1.735 and 2.125 eV, respectively (Figure 5b). By comparison, it is easy to find that the conjugated polyene is more likely to move in the direction of [1$\bar{1}$0]. Moreover, there is no significant correlation between the chain length and migration energy barrier in the [1$\bar{1}$0] direction when the chain length grows over a threshold, *e.g.*, by comparing C_8H_{10} and $C_{10}H_{12}$. This calculation implies that the formation of PA is the result of the collision coupling of the polyenes moving in the [1$\bar{1}$0] direction. Since the migration barrier along the [001] direction is much higher than that along the [1$\bar{1}$0] direction, only the migration of the monomer in the same and the most closed spine in the [1$\bar{1}$0] direction can contribute to polymerization, resulting in successful surface coverage modulation for suppressing defects.

4 Conclusions

In conclusion, we achieved the coupling of polyenes that are transformed from *n*-$C_{32}H_{66}$ on a Cu (110) surface under mild conditions and identified three distinct types of linkages by means of STM and nc-AFM with chemical bond resolution. The α-type linkage is the stemless coupling of the terminal C–C double bond in the *trans*-configuration, while β- and γ-type linkages present C–C coupling in *cis*-configurations. The in-depth elucidation enables us to regulate the ratios between different linkages and suppress the β- and γ-type connections by modulating the surface coverage, which may in general pave the way towards the further understanding and controlling uniform products in on-surface chemistry and might be particularly interesting for alkane chemistry.

Acknowledgements This work was financially supported by the National Natural Science Foundation of China (21790053, and 51821002) and the Ministry of Science and Technology (2017YFA0205002). We also thank the Collaborative Innovation Center of Suzhou Nano Science & Technology, the Priority Academic Program Development of Jiangsu Higher Education Institutions (PAPD), and the 111 project.

Conflict of interest The authors declare no conflict of interest.

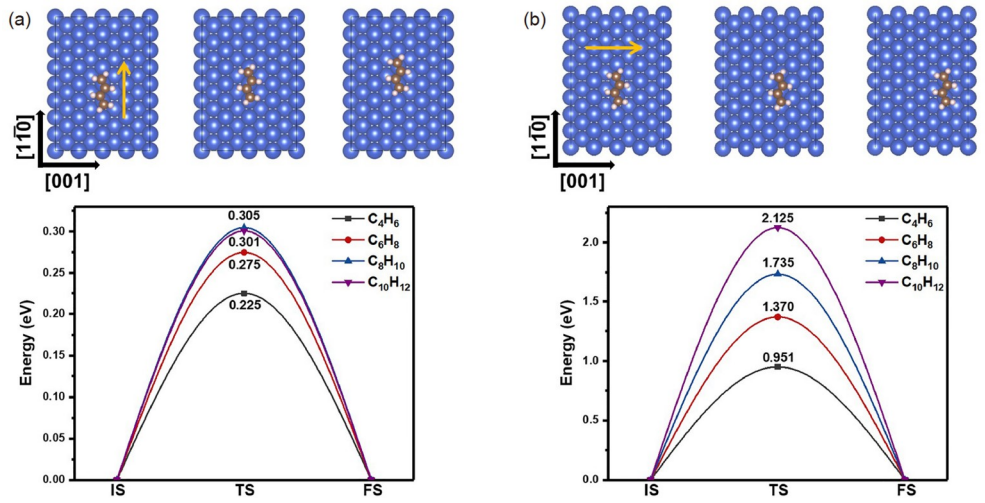

Figure 5 Migration energy diagram of polyenes with different chain lengths in different directions on the Cu (110) surface. (a) The migration barriers of C_4H_6, C_6H_8, C_8H_{10}, and $C_{10}H_{12}$ along the [1$\bar{1}$0] direction. (b) The migration barrier of C_4H_6, C_6H_8, C_8H_{10}, and $C_{10}H_{12}$ along the [001] direction (color online).

Supporting information The supporting information is available online at http://chem.scichina.com and http://link.springer.com/journal/11426. The supporting materials are published as submitted, without typesetting or editing. The responsibility for scientific accuracy and content remains entirely with the authors.

1 Sichel EK, Rubner MF. *J Polym Sci Polym Phys Ed*, 1985, 23: 1629–1636
2 Shirakawa H, Ito T, Ikeda S. *Polym J*, 1973, 4: 460–462
3 Heeger AJ. *Angew Chem Int Ed*, 2001, 40: 2591–2611
4 Springborg M. *Phys Rev B*, 1986, 33: 8475–8489
5 Audenaert M, Gusman G, Deltour R. *Phys Rev B*, 1981, 24: 7380–7382
6 Schen MA, Lefrant S, Perrin E, Chien JCW, Mulazzi E. *Synth Met*, 1989, 28: D287–D294
7 Schen MA, Chien JCW, Perrin E, Lefrant S, Mulazzi E. *J Chem Phys*, 1988, 89: 7615–7620
8 Soga K, Kawakami S, Shirakawa H, Ikeda S. *Makromol Chem Rapid Commun*, 1980, 1: 523–526
9 Chien JCW, Capistran JD, Karasz FE, Dickinson LC, Schen MA. *J Polym Sci B Polym Lett Ed*, 1983, 21: 93–97
10 Brédas JL, Chance RR, Silbey R, Nicolas G, Durand P. *J Chem Phys*, 1981, 75: 255–267
11 Hoffman DM, Gibson HW, Epstein AJ, Tanner DB. *Phys Rev B*, 1983, 27: 1454–1457
12 Yoshino K, Hayashi S, Inuishi Y, Hattori K, Watanabe Y. *Solid State Commun*, 1983, 46: 583–585
13 Bechtold G, Genzel L, Roth S. *Solid State Commun*, 1985, 53: 1–3
14 Langer JJ. *Synth Met*, 1986, 16: 317–323
15 Wallace DS, Stoneham AM, Hayes W, Fisher AJ, Testa A. *J Phys-Condens Matter*, 1991, 3: 3905–3920
16 Shirakawa H. *Angew Chem Int Ed*, 2001, 40: 2574–2580
17 Ramachandran GK, Tomfohr JK, Li J, Sankey OF, Zarate X, Primak A, Terazono Y, Moore TA, Moore AL, Gust D, Nagahara LA, Lindsay SM. *J Phys Chem B*, 2003, 107: 6162–6169
18 Osuka A, Yamada H, Shinoda S, Nozaki K, Ohno T. *Chem Phys Lett*, 1995, 238: 37–41
19 Chen J, Reed MA, Rawlett AM, Tour JM. *Science*, 1999, 286: 1550–1552
20 Zhong Q, Hu Y, Niu K, Zhang H, Yang B, Ebeling D, Tschakert J, Cheng T, Schirmeisen A, Narita A, Müllen K, Chi L. *J Am Chem Soc*, 2019, 141: 7399–7406
21 Sun Q, Cai L, Wang S, Widmer R, Ju H, Zhu J, Li L, He Y, Ruffieux P, Fasel R, Xu W. *J Am Chem Soc*, 2016, 138: 1106–1109
22 Gao HY, Wagner H, Zhong D, Franke JH, Studer A, Fuchs H. *Angew Chem Int Ed*, 2013, 52: 4024–4028
23 Zhang YQ, Kepčija N, Kleinschrodt M, Diller K, Fischer S, Papageorgiou AC, Allegretti F, Björk J, Klyatskaya S, Klappenberger F, Ruben M, Barth JV. *Nat Commun*, 2012, 3: 1286
24 Yang B, Cao N, Ju H, Lin H, Li Y, Ding H, Ding J, Zhang J, Peng C, Zhang H, Zhu J, Li Q, Chi L. *J Am Chem Soc*, 2019, 141: 168–174
25 Bebensee F, Bombis C, Vadapoo SR, Cramer JR, Besenbacher F, Gothelf KV, Linderoth TR. *J Am Chem Soc*, 2013, 135: 2136–2139
26 Ji P, MacLean O, Galeotti G, Dettmann D, Berti G, Sun K, Zhang H, Rosei F, Chi L. *Sci China Chem*, 2021, 64: 636–641
27 Jiang L, van Deursen PMG, Arjmandi-Tash H, Belyaeva LA, Qi H, He J, Kofman V, Wu L, Muravev V, Kaiser U, Linnartz H, Hensen EJM, Hofmann JP, Schneider GF. *Sci China Chem*, 2021, 64: 1047–1056
28 Sun K, Chen A, Liu M, Zhang H, Duan R, Ji P, Li L, Li Q, Li C, Zhong D, Müllen K, Chi L. *J Am Chem Soc*, 2018, 140: 4820–4825
29 Li Q, Yang B, Lin H, Aghdassi N, Miao K, Zhang J, Zhang H, Li Y, Duhm S, Fan J, Chi L. *J Am Chem Soc*, 2016, 138: 2809–2814
30 Li X, Niu K, Zhang J, Yu X, Zhang H, Wang Y, Guo Q, Wang P, Li F, Hao Z, Xu C, Tang Y, Xu Z, Lu S, Liu P, Xue G, Wei Y, Chi L. *Natl Sci Rev*, 2021, 8: nwab093
31 Zhong D, Franke JH, Podiyanachari SK, Blömker T, Zhang H, Kehr G, Erker G, Fuchs H, Chi L. *Science*, 2011, 334: 213–216
32 Zhou X, Wang C, Zhang Y, Cheng F, He Y, Shen Q, Shang J, Shao X, Ji W, Chen W, Xu G, Wu K. *Angew Chem Int Ed*, 2017, 56: 12852–12856
33 Zhang J, Chang CR, Yang B, Cao N, Peng C, Zhang H, Tang DTD, Glorius F, Erker G, Fuchs H, Li Q, Chi L. *Chem Eur J*, 2017, 23: 6185–6189
34 Gong Z, Yang B, Lin H, Tang Y, Tang Z, Zhang J, Zhang H, Li Y, Xie Y, Li Q, Chi L. *ACS Nano*, 2016, 10: 4228–4235
35 Horcas I, Fernández R, Gómez-Rodríguez JM, Colchero J, Gómez-Herrero J, Baro AM. *Rev Sci Instruments*, 2007, 78: 013705
36 Bartels L, Meyer G, Rieder KH. *Appl Phys Lett*, 1997, 71: 213–215
37 Kresse G, Furthmüller J. *Comput Mater Sci*, 1996, 6: 15–50
38 Kresse G, Furthmüller J. *Phys Rev B*, 1996, 54: 11169–11186
39 Kresse G, Hafner J. *Phys Rev B*, 1993, 47: 558–561
40 Perdew JP, Burke K, Ernzerhof M. *Phys Rev Lett*, 1997, 78: 1396
41 Grimme S, Antony J, Ehrlich S, Krieg H. *J Chem Phys*, 2010, 132: 154104
42 Blöchl PE. *Phys Rev B*, 1994, 50: 17953–17979
43 Kresse G, Joubert D. *Phys Rev B*, 1999, 59: 1758–1775
44 Henkelman G, Jónsson H. *J Chem Phys*, 2000, 113: 9978–9985
45 Henkelman G, Uberuaga BP, Jónsson H. *J Chem Phys*, 2000, 113: 9901–9904
46 Rong ZY, Kuiper P. *Phys Rev B*, 1993, 48: 17427–17431
47 Kobayashi K. *Phys Rev B*, 1996, 53: 11091–11099
48 Mao J, Zhang H, Jiang Y, Pan Y, Gao M, Xiao W, Gao HJ. *J Am Chem Soc*, 2009, 131: 14136–14137
49 Wang S, Sun Q, Gröning O, Widmer R, Pignedoli CA, Cai L, Yu X, Yuan B, Li C, Ju H, Zhu J, Ruffieux P, Fasel R, Xu W. *Nat Chem*, 2019, 11: 924–930
50 Shirakawa H. *Curr Appl Phys*, 2001, 1: 281–286